SUBCONTRACT TITLE**:** **Fabrication and Physics of CdTe Devices by Sputtering**

SUBCONTRACT TITLE**:** **ZXL-5-44205-01**

QUARTERLY TECHNICAL STATUS REPORT FOR**:**

Phase 3/Quarter 3

SUBMITTED TO**:** **Bolko von Roedern**
National Renewable Energy Laboratory

PRINCIPAL INVESTIGATORS:

A.D. Compaan (P.I.), R.W. Collins, V.G. Karpov
Department of Physics and Astronomy
Dean Giolando, Dept. of Chemistry
The University of Toledo
Toledo, OH 43606

This progress report covers the Third Quarter of Phase 3 for the period from December 01, 2007 through March 31, 2008, of the above Thin Film Photovoltaic Partnership Program subcontract. This report will present 1) properties of phosphorus-doped CdTe films prepared by sputtering from pressed targets of CdTe and Cd_3P_2, 2) optimization studies on ultra-thin CdS/CdTe cells with efficiencies exceeding 10% for 0.5μm CdTe, and 3) results of electrochemical treatment with polyaniline of pinholes in CdTe devices.

1 Study of Phosphorus Doped CdTe Film

1.1 Introduction

One major effort in this phase was to reach significant p-type doping in CdTe through the incorporation of phosphorous during sputtering. Control of p-type doping in CdTe has been difficult and this study indicates that large quantities of phosphorous may be needed. However we have some evidence that it may be possible to control the thickness of the depletion region in the CdTe layer and increase the built-in electric field with doping from sputtering using targets with cold-pressed mixtures of CdTe and Cd_3P_2.

One pure CdTe and three P-doped CdTe targets were pressed at UT with three different P densities, as summarized in Table 1.1. The three P-doped CdTe targets were pressed from a mixture of Cd_3P_2 powder with CdTe powder. The Cd_3P_2 powder was supplied by Alfa Aesar with purity of 99.5% and grain size -100 Mesh (< 150μm). The total metal-based impurity level is 0.25%, including Sn, Al, Ni, Zn and etc. The purity of CdTe is 99.999% with grain size -16 Mesh (< 1.2mm). The mixed CdTe and Cd_3P_2 powders were further ground in a mortar and pestle. The powder mixture was then compressed in a stainless steel cup under a compression force of 1900 pounds/inch^2 for duration of at least 10 minutes. The homemade pure CdTe target was pressed in the same way except for grinding.

CdTe films sputtered from P-doped CdTe targets onto aluminosilicate glass at 250°C were studied together with films from pure CdTe targets deposited at the same condition and onto the same type of substrate. We report here the characterization of the thin films using SEM, EDX, XRD, hot probe, and strip line resistivity. Cell performance will be reported later.

For comparison, we fabricated complete cells with sputtered film from the homemade pure CdTe target as well as the doped targets. Efficiencies of the pure CdTe cells on TEC7 glass have been measured to be 11 ~ 12%, similar to our standard cells sputtered from commercial sintered CdTe targets.

Table 1.1 Compressed targets made of CdTe and CdTe/Cd_3P_2 mixture

Target No.	CdTe (g)	Cd_3P_2 (g)	P density (weight)
1	31.4	0.0	0.0%
2	34.0	0.2	0.09%
3	15.0	2.0	1.63%
4	30.7	4.1	1.82%

1.2 Film Morphology Study by XRD, SEM, EDX

1.2.1 SEM and EDX studies

Scanning electron microscopy (SEM) images and energy dispersive x-ray spectroscopy (EDX) spectra from the films sputtered from the 1.8% P-doped CdTe target were collected at the Electron Microbeam Analysis Laboratory (EMAL) of the University of Michigan, using an FEI Nova Nanolab Dualbeam workstation.

SEM images of the as-grown, $CdCl_2$-treated and Ar-annealed CdTe:P films are presented in Figure 1.1. The as-grown CdTe:P film shows distinct grains with well-defined facets. The $CdCl_2$-treated film was partially covered with 20nm of evaporated Au for better SEM image quality. Due to the high resistivity of this film (section 1.3), the SEM image is always distorted by the electric fields from electron accumulation during scans. There is little indication of recrystallization occurring during the chloride treatment. Indeed, grain boundary gaps widen to

approximately 30 nm around all the grains probably due to loss of P, Cd and/or Te, instead of grain coalescence after chloride treatment as usually observed in CdTe film. However, after annealing in Ar there is considerable fusing of grains. Grain boundaries are much less distinct. Voids of ~40nm can also be observed.

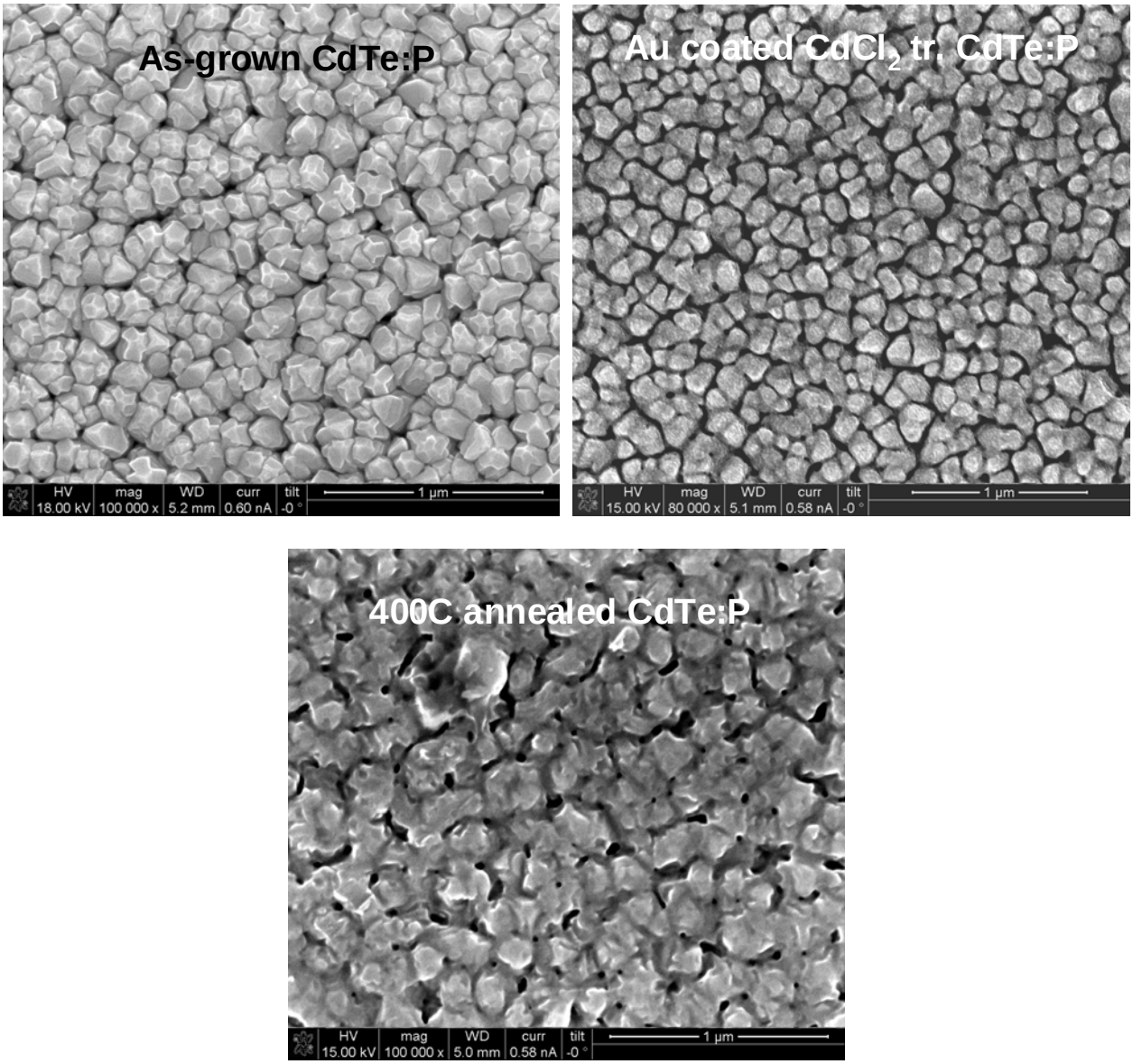

Figure 1.1 SEM images of as-grown, chloride-treated and Ar-annealed CdTe:P from the 1.8% P-doped CdTe target (No. 4).

Table 1.2 Grain size and P density of CdTe:P film sputtered from 1.8% target.

Sample ID	treatment	Grain size (nm)	Wt. % of P
ssc219b	as-grown	120 ± 10	0.3 ± 0.2
ssc219a	Std. $CdCl_2$ treatment	150 ± 15	0.3 ± 0.2
ssc219c	400°C Ar annealing	230 ± 5	0.4 ± 0.2

Grain size, calculated by dividing the length of the line drawn across the SEM micrograph by the number of grains intersected by the line, is the same for the as-grown and chloride-treated films. Yet, the grain size of the Ar annealed film increases to 230 nm, almost double that of the other two films.

EDX spectra were also collected. We used either 18 or 15 keV electron beams with beam current of 0.6nA for excitation. For comparison, the spectra have been normalized to the maximum peak intensity of Cd $L_{\alpha 2}$. The spectra of as-grown and $CdCl_2$–treated films are identical except for the presence of the Cl K_α peak at 2620 eV in the latter one. This is from residual $CdCl_2$ mostly on the film surface. The weak P $K_{\alpha 1,2}$ (2013 eV) peak appearing in all three samples, as shown in Figure 1.2, indicates likely successful phosphorus doping in these CdTe films sputtered from the 1.8% P-doped CdTe target, although EDX cannot distinguish doping from the presence of elemental P. Quantitative analysis indicates approximately 0.3 Wt% of phosphorus, as listed in Table 1.2. Due to the low intensity of this peak, it is hard to determine whether there is any variation of phosphorus density after different treatments.

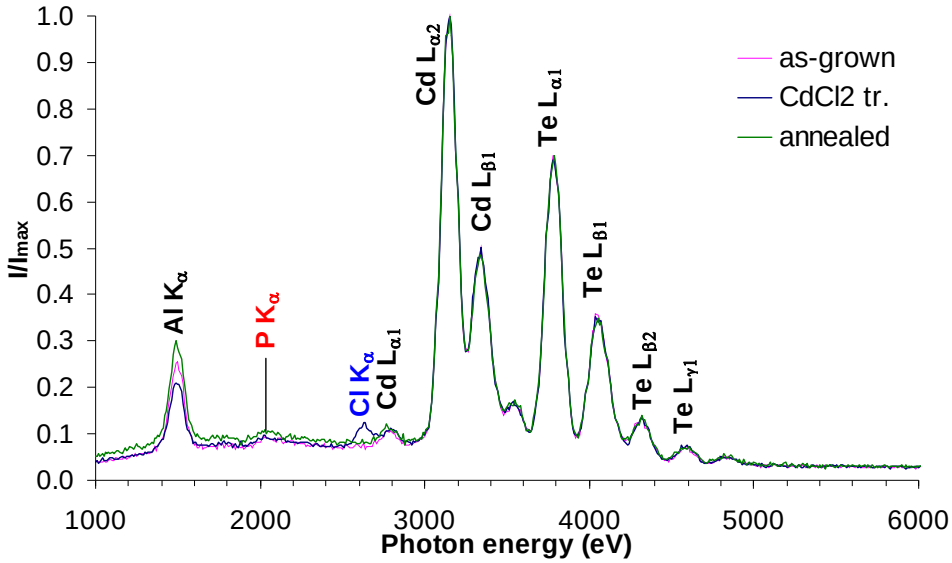

Figure 1.2 EDX spectra of as-grown, standard $CdCl_2$ treated and Ar annealed CdTe:P films. The P $K_{\alpha 1,2}$ peaks at 2013 eV in all the three films confirm existence of phosphorus dopant.

Analysis of phosphorus density in the same CdTe films from 1.8% P-doped target has been investigated by inductively coupled plasma analysis (ICP) and phosphorus peaks are confirmed, but the ICP data are not yet quantified.

1.2.2 XRD studies

Films sputtered from pure CdTe, 1.6% and 1.8% phosphorus targets were deposited on aluminosilicate glass. Some films were also activated in a mixture of dry air and $CdCl_2$ vapor at 387 $^\circ$C for 30 minutes – our standard condition. One piece of the film sputtered from CdTe target No. 4 with 1.8% P was also annealed in Ar at 400 $^\circ$C for 40 minutes with a proximity cap of intrinsic CdTe film. High purity Ar (99.999%) flowed through the glass tube at 25 ml/minute during the annealing. The film thicknesses and treatment are summarized in Table 1.3.

XRD was performed at the Instrumentation Center at the University of Toledo on a PANalytical X'Pert Pro system. Films before and after chloride treatment as well as the Ar-annealed film were scanned with resolution of 0.017°, as shown in Figure 1.3. The most apparent effect of the P dopant on the XRD spectra of CdTe is the reduced random orientation with increasing P density. The intensity ratio of the CdTe (220) and (110) peaks increases from 0.11 to 0.5 after chloride treatment for the intrinsic film. For the film sputtered from 0.09% P-doped CdTe target, this intensity ratio starts with 0.037 (one third of intrinsic film) in as-grown film and increases to 0.046 (one tenth of intrinsic film) after treatment. Moreover, in CdTe film grown from 1.8% target, peaks other than the (111) are basically undetectable from all of the as-grown, chloride treated and Ar annealed films, except for the (511) peak (Figure 1.3d). To emphasize this phenomenon, the spectra of the CdTe:P films from 1.8% target are plotted in logarithmic scale as shown in Figure 1.3d. The peak intensity ratios of (220) to (110) are in the 10^{-4} range. The mechanism of this phenomenon is unknown yet.

Table 1.3 Summary of single layer CdTe:P films on aluminosilicate glass

Target (P density)	Film thickness (μm)	Sample ID	treatment	XRD peak intensity ratio (220)/(111)*	FWHM of (111)
No.1 – 0.0%	2.0	ssc738	as-grown	0.11	0.24°
		ssc738Cl	Std. $CdCl_2$ treatment	0.50	0.09°
No.2 – 0.09%	2.0	ssc747	as-grown	0.037	0.20°
		ssc747Cl2	Std. $CdCl_2$ treatment	0.046	0.12°
No.4 – 1.82%	1.9	asc219b	as-grown	$< 2\times10^{-4}$ *	0.11°
		asc219a	Std. $CdCl_2$ treatment	$< 2\times10^{-4}$ *	0.10°
		asc219c	400°C Ar annealing	$< 4\times10^{-4}$ *	0.12°

* CdTe (220) peak intensities are at the background noise level.

Evidence of recrystallization of CdTe in the $CdCl_2$ treated samples is clear in the intrinsic films and the ones from the 0.09% target, since the intensities of all the peaks increase and the FWHMs decrease after chloride treatment, as shown in Figure 1.3. The most interesting result in XRD is the narrow (111) peak observed in the "as-grown" CdTe:P film from the 1.8% target. The FWHM of this as-grown film is 0.11° and remains the same after both chloride treatment and Ar annealing, which is similar to that of undoped films after chloride treatment (Table 1.3). The CdTe (111) peak intensity does not change much after chloride treatment and Ar annealing, instead of increasing as in the undoped film, as shown in Figure 1.3c. This indicates better crystalline structure quality grown during deposition with the presence of phosphorus. SEM images of the CdTe:P film from the 1.8% target also confirms high quality polycrystalline gains in the as-grown film, as discussed in the next section. This unusual behavior seems to point to the high phosphorous density (~1%) facilitating grain growth in a manner somewhat similar to $CdCl_2$. This behavior and the doping effects are being investigated further.

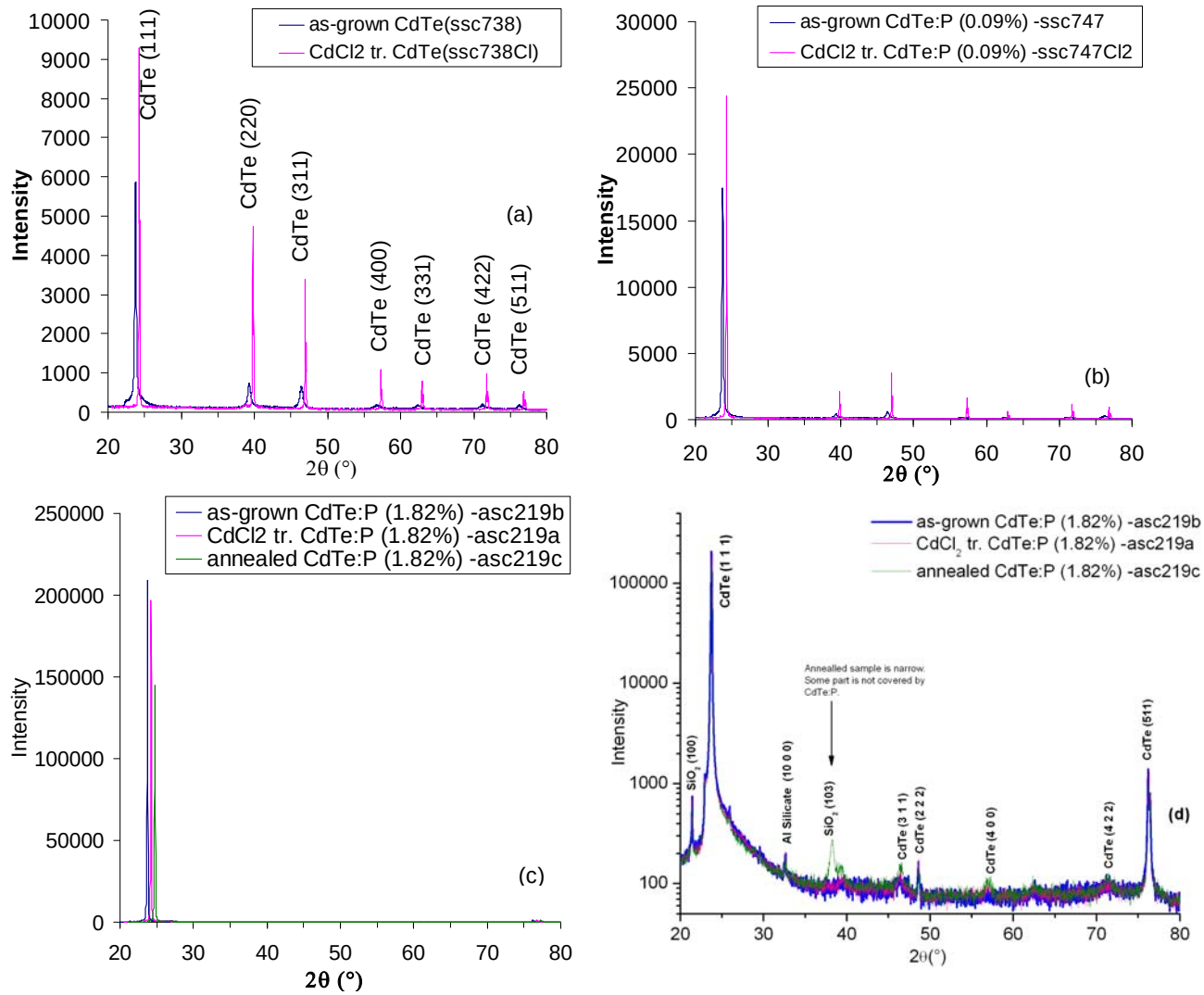

Figure 1.3 XRD of CdTe and CdTe:P films sputtered from (a) pure CdTe target, (b) CdTe target with 0.09% P and (c),(d) CdTe target with 1.82% P. XRD of both as-grown and vapor $CdCl_2$ treated films are plotted. For film from target of 1.82% P, XRD of Ar-annealed film is also plotted in Fig. (c) and (d). For comparison, spectra of chloride treated films are intentionally shifted with 0.5° in (a), (b) and (c). The one of Ar annealed in (c) is shifted by 1°. Note log scale in Fig. d.

1.3 Electrical Properties – Resistivity and Dopant Type

The most interesting properties of these phosphorus doped CdTe films are the improved conductivity and the light sensitive conductivity of the heavily doped films.

The sheet resistance was measured in a strip-line geometry. Gold contact lines with gradually increased separation were evaporated onto the surface of the films with thickness of around 40nm. The width and length of the gold lines are 1.14 and 7.54 mm, respectively. Resistance - R across adjacent lines was measured as a function of the line separation (L_i) by a Keithley 617 electrometer with high input impedance and measurement limit up to $2\times10^{11}\Omega$. Sheet resistance per unit length of the contact line was computed as the slope of $R(L_i)$.

Resistivity was then computed and listed for different films in Figure 1.4 and plotted in Figure 1.4. Both dark and light (1 sun Xe arc lamp) resistivity were measured.

Table 1.4 Measured resistivity of CdTe:P films in strip line geometry.

P in targets / measurement	as-grown (Ω*cm)	light/dark	$CdCl_2$ treated (Ω*cm)	light/dark	Ar annealed (Ω*cm)	light/dark
0.0% P (dark)	$>1.0\times10^{9}$		$3.3\pm0.2\times10^{7}$	5.8×10^{-4}		
0.0% P (1 sun)	N/A		1.9×10^{4}			
0.09% P (dark)	$3.1\pm0.1\times10^{8}$		$3.4\pm1.0\times10^{7}$	2.5×10^{-4}		
0.09% P (1 sun)	N/A		$8.5\pm0.6\times10^{3}$			
1.82% P (dark)	$1.16\pm0.08\times10^{5}$	0.1	$1.6\pm0.2\times10^{8}$	4.8×10^{-4}	$4.82\pm0.07\times10^{7}$	1.4×10^{-4}
1.82% P (1 sun)	$1.14\pm0.02\times10^{4}$		$7.7\pm0.4\times10^{4}$		$6.7\pm0.2\times10^{4}$	

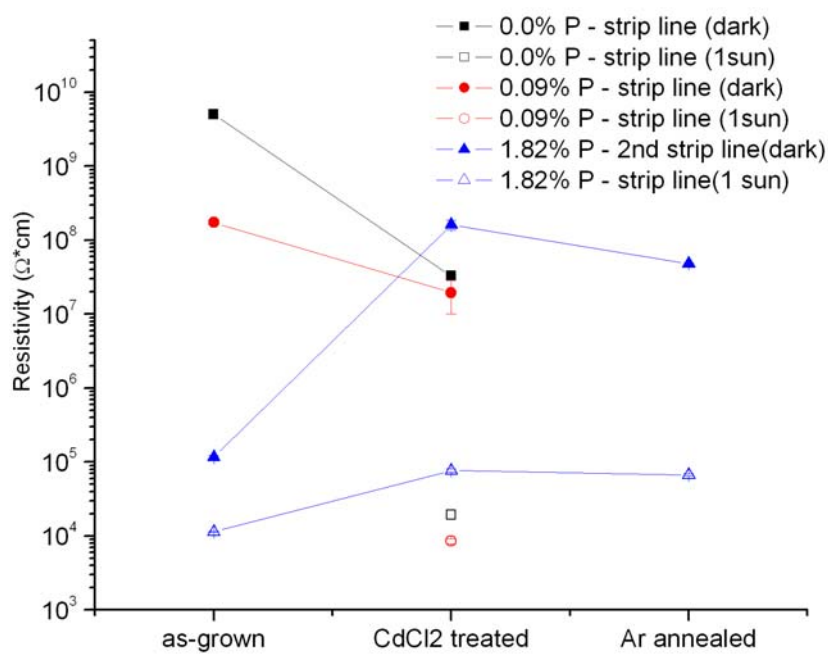

Figure 1.4 (The as-grown intrinsic CdTe film is plotted at 5×10^{9} Ω*cm as a representative value $> 1.0\times10^{9}$ Ω*cm.)

The sheet resistance of the as-grown undoped CdTe film is higher than the measurement capability of the Keithley 617 and the estimated resistivity is greater than $1.0\times10^{9}\Omega$. Other films which are measured with resistivity above 10^{7} Ω*cm have large resistance at each measurement point and are sensitive to charging or discharging current to capacitance in circuit. Long acquisition time occasionally up to 2 hours was needed for stable readout.

A general trend in as-grown films is that the resistivity is found to decrease with increasing phosphorus density. The resistivity of the film from the 1.8% target decreases *three orders of magnitude* compared to the one from 0.09% target (Table 1.4). Yet in the chloride-treated films, the resistivity increases with phosphorus density. For undoped CdTe films and the ones from 0.09% target, the chloride treated films are more conductive than untreated ones. However, in

the CdTe:P film from the 1.8% target after chloride treatment or Ar annealing, the resistivity increased to the same order of magnitude as for undoped films and the one from 0.09% target. This is consistent with the image distortion observed in SEM images from the two samples (not shown).

Another interesting feature we observed during measurement is the photoconductivity of the films. Light resistivity under one sun of the as-grown film from 1.8% target was measured to be 1.14×10^4 Ω*cm, one order of magnitude lower than the dark resistivity. For the as-grown intrinsic films and the ones from 0.09% target, no reasonable data could be obtained under one sun illumination. For chloride treated films with different P density, similar photo-sensitive behavior was observed under light. Resistivity of all the chloride-treated films with different P density drops three orders of magnitude from the value in dark (Figure 1.4).

Hot Probe measurements were employed to study the carrier type in as-grown films sputtered from target No.3 and 4 on aluminosilicate substrates. Higher electric potential is always observed on the cold probe indicating holes as the majority carrier in the CdTe:P films.

2 Optimization of Ultra-Thin CdS/CdTe cells

In this section we highlight our efforts in fabrication of high efficiency ultra-thin CdS/CdTe cells. Our previous experience suggests that there are several aspects that are critical for devices with ultrathin (less than 0.5 micron) layers. In general the devices are similar to those of UT standard 2.5 micron CdTe devices although the process window appears to be higher for the thicker cells. Below we summarize these challenges along with our strategies to overcome them and recent results on ultra-thin cells that we have achieved.

2.1 Reliable pinhole-free deposition process

We have reported previously that pinhole density appears to be a function of the chamber maintenance schedule. Specifically, the highest pinhole density was routinely observed immediately after the cleaning of the ground shield. Our explanation, based on the measurement of the substrate self-bias potential, suggested that the reason for the pinhole appearance is the negative substrate self bias which is typical for our system when the ground shield surface is clean and highly conductive. It was suggested that those conditions are unfavorable presumably due to positively charged particles inside the chamber that get attracted to a negatively biased substrate.

It has also been found that after a number of depositions without ground shield cleaning the plasma potential changes and so does the substrate self bias, becoming less negative and eventually positive. Simultaneously the observed pinholes density decreases and eventually becomes low enough not to affect the device yield substantially.

Based on these observations we revised our chamber cleaning policies to clean the loose particles leaving a solid CdTe coating on the ground shield intact. As a result we have been able to deposit ultra-thin CdTe cells with a very low pinhole density.

2.2 Use of front buffer layer due to a possible shorting via weak diodes

It has been shown in [1] that even in the absence of physical pinholes the performance of the thin CdTe devices may suffer due to the weak diodes. It has also been suggested that using HRT-coated TCOs is likely to improve the situation. In our current work we use HRT-coated TCO glass and we see a significant improvement for the devices with thin CdS/CdTe layers. We

found the difference in the performance of the cells with and without a very thin (below 50 nm) CdS layer on the substrates with and without HRT-coating to be one of the strongest indications of the HRT layer quality (Figure 1.) For that test we used a standard 2.5 micron CdTe layer cells since the baseline is well established and results can be interpreted more easily. It can be seen from the Figure 2.1 that the significant difference between the cells grown on bare and HRT-coated TCOs is mainly due to the difference in open-circuit voltage and is significant enough to see the difference between the substrates. Statistic is given for the ensemble of 35 cells of each type with contact area of 0.06 cm^2. Box indicates ±50% and whisker indicates extremes at 75% and 25%. That applies to all the "box and whiskers" plots in this section.

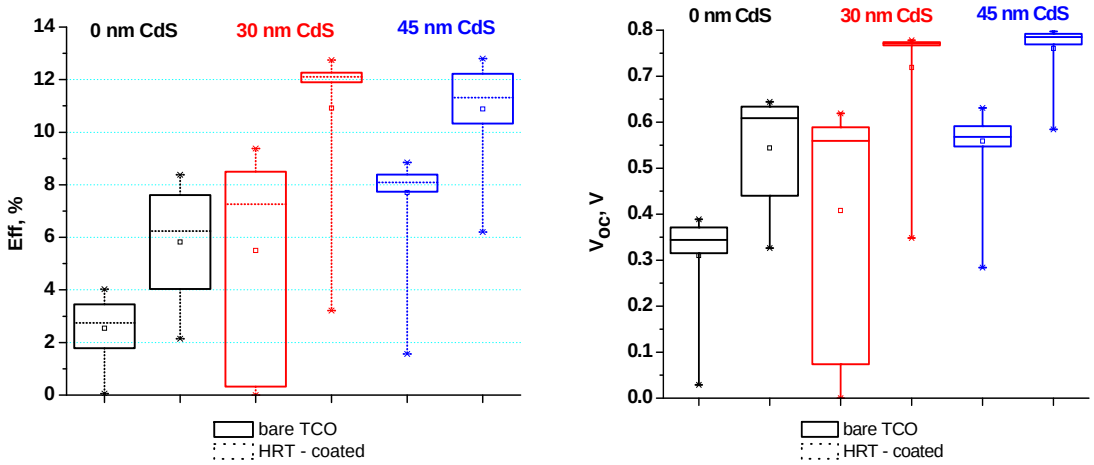

Figure 2.1. Difference in efficiency and V_{oc} of the dot cells grown on bare (solid) and HRT-coated TCOs. (CdTe thickness ~ 2.4 µm.)

2.3 Optimized CdS thickness

It has been reported previously that for standard 2.4 micron CdTe UT cells the optimal thickness of the CdS layer is within the range of 80 nm to 100 nm. Thinning the layer further down below 80 nm leads to efficiency losses due to decrease of V_{oc} and FF. On the other hand making the layer thicker than 100 nm does not lead to increase of these parameters while J_{sc} keeps decreasing due to the optical losses in the window layer. Application of the HRT coating allows us to reduce the thickness of the CdS layer to about 30 nm without any significant loss of V_{oc}, FF or device yield while helping to gain from 2 to 3 mA/cm^2 of J_{sc} due to increased transmission in the blue. This, of course, has been observed earlier by several other groups using other deposition methods, but it is our first systematic study of this dependence. This is particularly important for the thin (less than 1 micron CdTe) cells that suffer from the deep penetration losses on the other side of the spectrum (Figure 2.2).

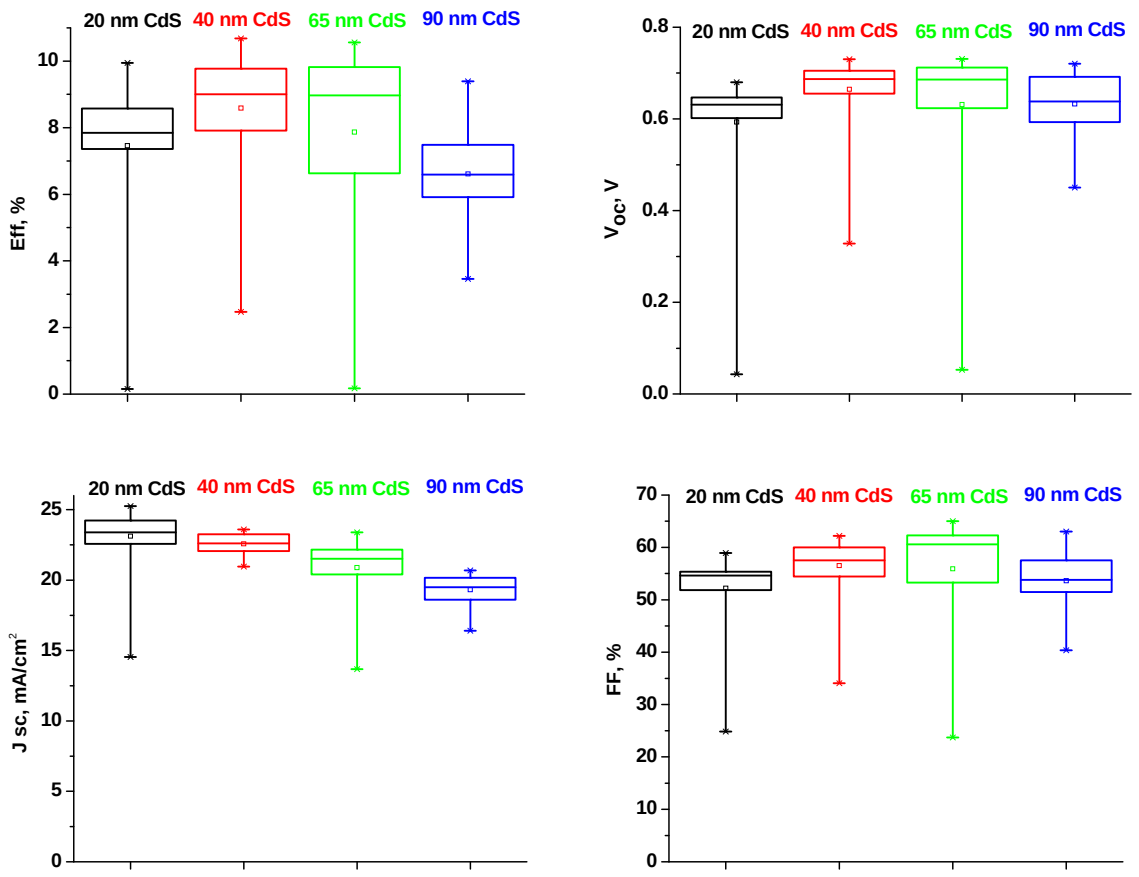

Figure 2.2. Effect of CdS layer thickness on cells with CdTe thickness ranging from 0.5 to 1.0 micron.

2.4 Optimized $CdCl_2$ treatment

The issue of optimizing $CdCl_2$ treatment conditions is extremely important in the case of thin CdTe cells. We have used wet $CdCl_2$ treatment instead vapor treatment for our recent thin cells since it provided better uniformity over the sample area and better control over the process. We also kept the temperature constant at 387 C and used the treatment time as the adjustable parameter since it scales more linearly with CdTe thickness. We are currently in the process of optimizing the treatment conditions and our preliminary results show that the treatment time should be about 3 minutes for the cells with a 0.5 micron CdTe layer. Treatment for twice as long yields less efficient cells on average as can be seen from the Figure 2.3 (compare solid and dot boxes), although the difference in the best out of 35 cells for each sample was relatively small and mainly due to the decrease in fill factor.

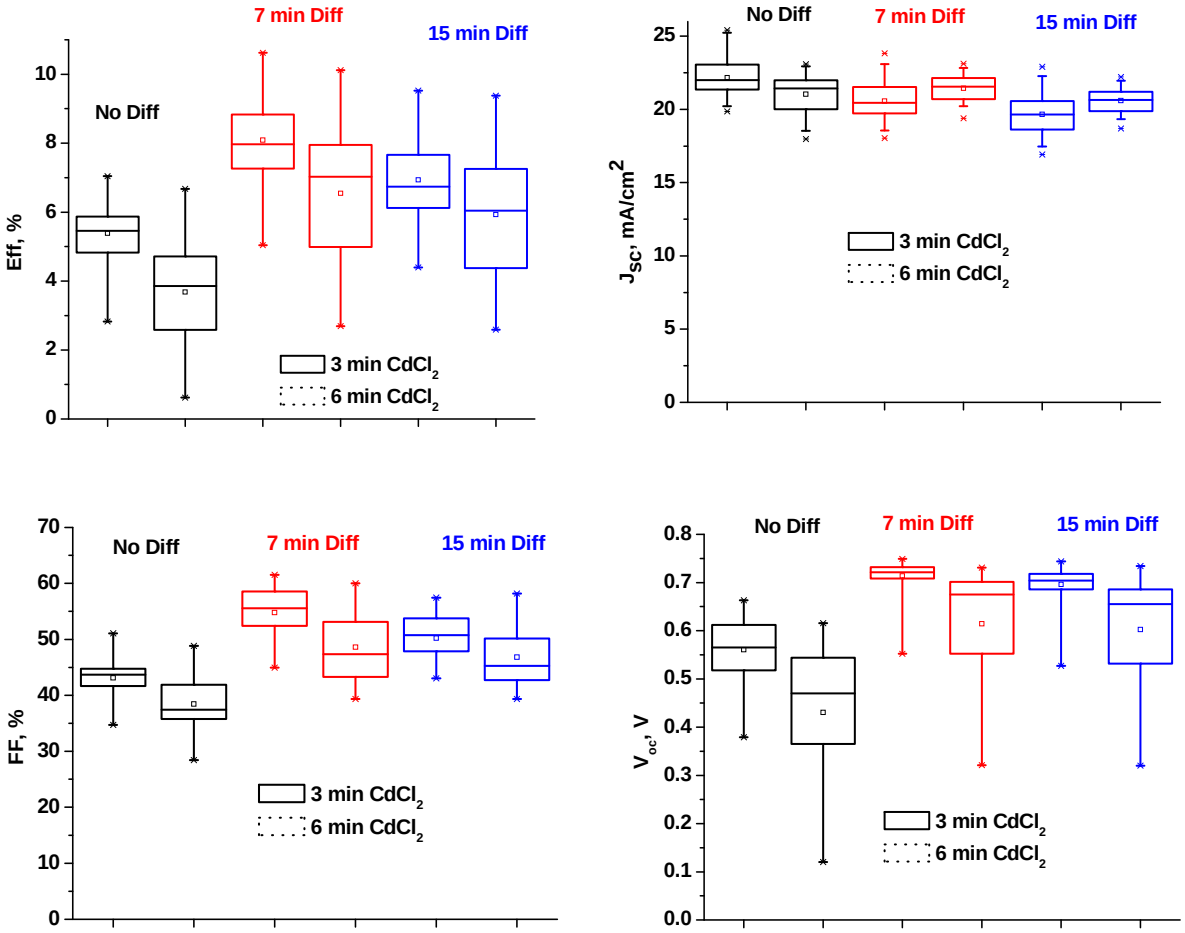

Figure 2.3. First and secondary metrics for the 0.5 micron CdTe cells as a function of $CdCl_2$ treatment time and Cu diffusion time. (Left/right data are for 3/6 minutes, respectively.)

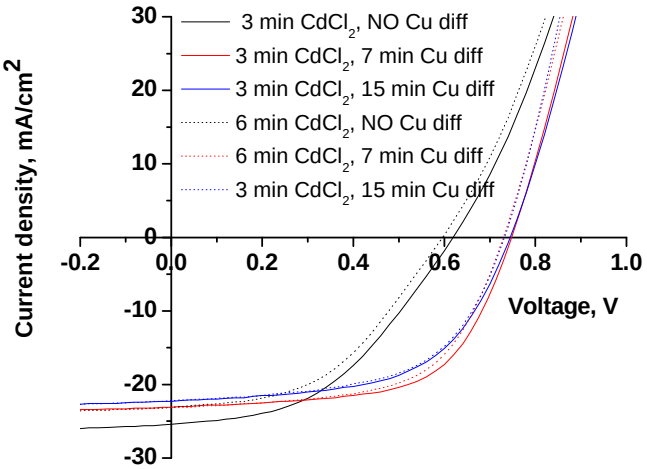

Figure 2.4. Best 0.5 micron CdTe cells as a function of $CdCl_2$ treatment time and Cu diffusion time.

2.5 Optimized Cu thickness and diffusion time

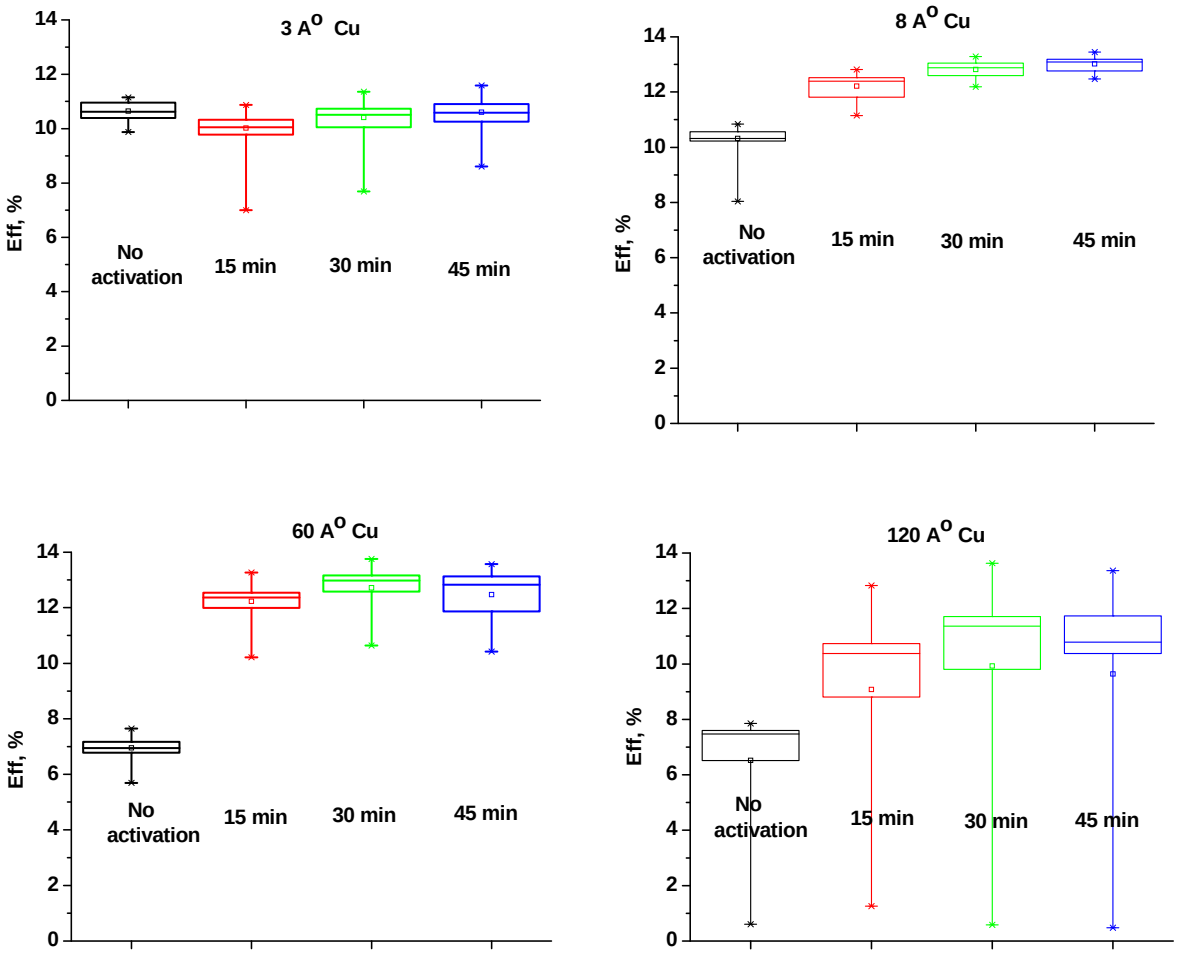

Figure 2.5. Cell efficiency dependence on the thickness of as-deposited Cu layer and heat treatment activation time. Cells are 30nm CdS/ 2.4 micron CdTe

Another extremely important parameter for the thin cell is the thickness of the as-deposited Cu layer in the standard UT Cu/Au evaporated back contact and the activation time required for that given thickness. We have previously studied the dependence of the standard (2.5 micron CdTe) cell performance on the Cu thickness and the heat treatment (at 150 ^{o}C) activation time (Figure 2.4.) over the wide range of Cu thickness (from 5 A to 120 A). There were 3 main observations made:

1) Unless the Cu layer thickness is extremely small (below 5 A) a controlled diffusion time is required to achieve optimum cell performance.
2) The thicker the as-deposited Cu layer the lower is the efficiency of the cells that did not receive any Cu activation treatment at all
3) The thicker the Cu layer, the steeper is the slope of the efficiency vs. activation time curve for the first 15 to 30 minutes of activation

4) If the Cu layer is extremely thin (below or about 5 A) there was no significant change in efficiency as a function of activation time observed (Figure 2.5 and Figure 2.6)

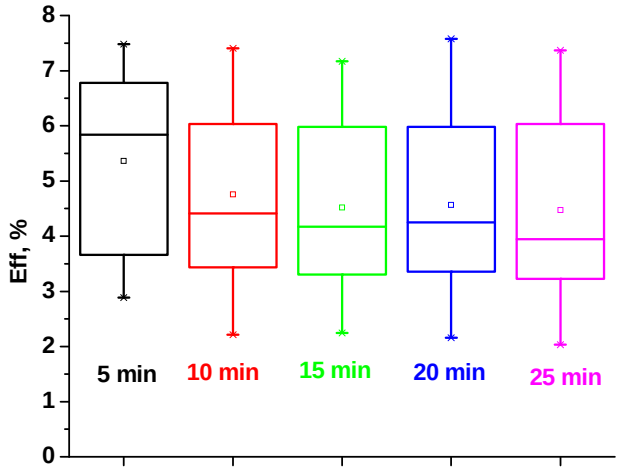

Figure 2.6. Efficiency of the 0.5 micron CdTe cells with 5 °A of as-deposited Cu vs. activation time

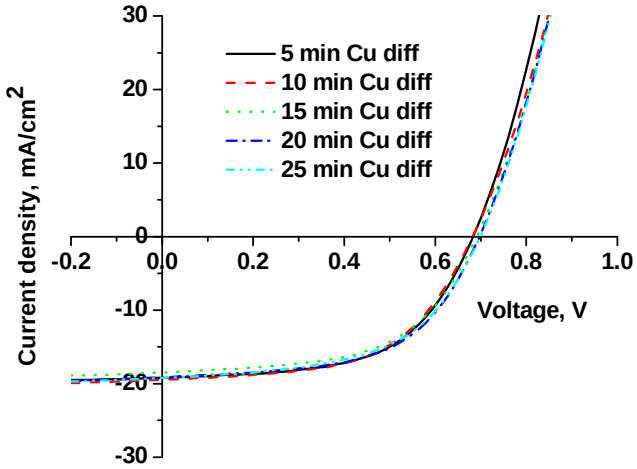

Figure 2.7. I-V curves of the best cells from the ensembles in Figure 6.

Another important observation that was made previously but not reflected in the graphs presented here is that use of our standard 30 A Cu back contact followed by the standard 45 minutes activation is not optimum for cells with less than 1 micron CdTe layers. Therefore our strategy based on the data available so far is to use a Cu layer with thickness in the 5 A to 10 A range followed by a shortened activation time of about 5 to 10 minutes that yielded the best result so far (10.5% cell for the 0.5 micron CdTe – see Figure 2.2.)

References

1. Y. Roussillon, V. G. Karpov, D. Shvydka, J. Drayton, and A. D. Compaan *Back contact and reach-through diode effects in thin-film photovoltaics*, J. Appl. Phys. December 01 (2004)

3 Electrochemical Treatment of pin-holes in CdTe Photovoltaic Device

Sputtered, thin-film CdTe devices having the structure glass/TCO/CdS/CdTe usually consist of fairly uniform and densely packed films of CdS and CdTe. However, on occasion, devices are obtained containing defects created during the fabrication process; such as non-uniformity, pinholes and porous material. The presences of these defects in the CdTe layer manifest themselves when the final metal electrode is deposited and the metal makes electrical contact with the TCO layer. This leads to the formation of a wire-like connection through the photovoltaic device (shunt), which adversely affects the overall performance of the solar cell. One solution is to selectively fill the pinholes and pores with a resistive material, such as polyaniline, using an electro-chemical polymerization technique. The goal is to selectively coat any portions of the TCO layer that are exposed through the semiconductor layers, without affecting the surface of the CdTe layer. After treatment an insulating material is expected to be on the TCO that will prevent the formation of an electrical contact between TCO and metal, during the metal deposition. For this project, a purposely made porous CdTe device was examined.

A freshly prepared solution containing 0.2 M Aniline, 0.1 M p-toluenesulfonic acid (p-TSA), 1.0 M sodium chloride in water was stirred for at least a half hour, providing a solution with a pH ~6.2. Since aniline is photo sensitive, the entire process was done inside a hood with the lights off. Aniline, and its solutions, oxidize on exposure to air (oxygen) and light, as seen by a change in color (changes color from colorless to dark brown).

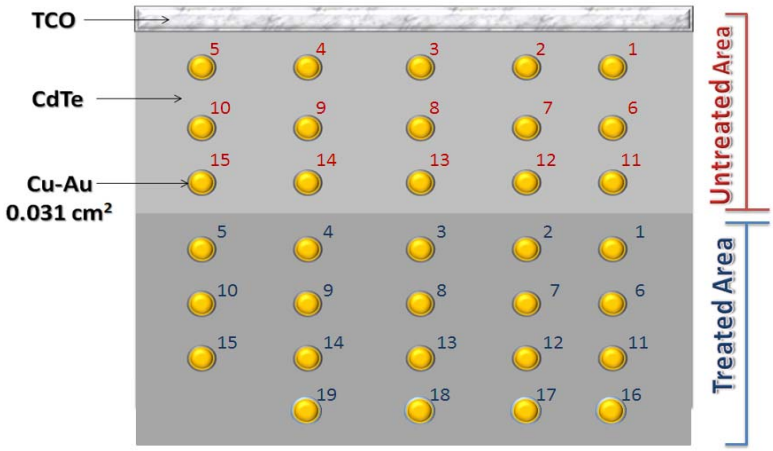

Figure 3.1 Top-view of a CdTe solar cell sample, which has been half treated using electrochemical polymerization technique.

Treatment experiment: - A potentiostat (D.C. power supply), containing two wires terminating with an alligator clip, was used to apply a potential to the TCO layer of a CdTe device and a platinum electrode was used as an auxiliary electrode. The TCO layer of the CdTe photovoltaic device acted as the cathode/positive electrode and the platinum electrode as the anode/negative. The electrodes where placed in a beaker filled with one inch height of the aniline solution. A voltage of 2.0 Volt was applied for 20 mins to polymerize the monomer. After the polymer treatment the device was rinsed, dried with a stream of compressed air and

then metalized using Cu-Au as a back contact (completing the solar cell) under standard conditions for the UT treatments. Characterization was in the form of IV-measurements.

The CdTe sample was cut from a 3 inch by 3 inch sample to 1 inch by 2 inch samples used for this study. As shown in Figure 3.1, 19 cells were devices treated using the electrochemical polymerization technique, while the other 15 cells were untreated devices used as controls. In Figure 3.2, 3.3, 3.4 and 3.5; the open-circuit voltage, short-circuit current, fill factor and efficiency respectively, of a total of these 34 complete cells (19 treated and 15 untreated/control) were measured.

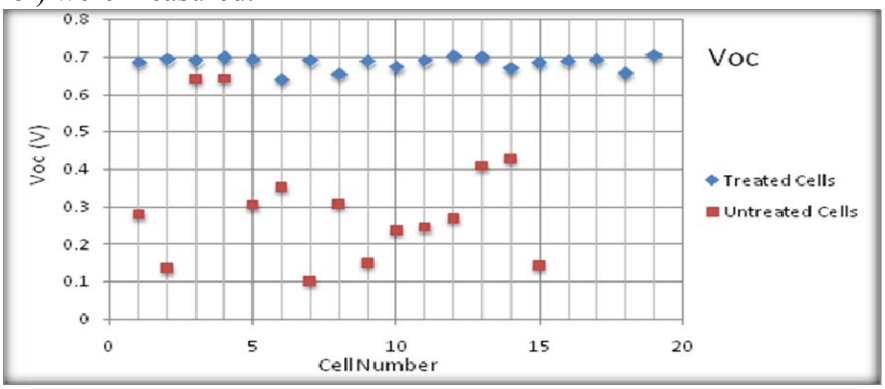

Figure 3.2 Open-Circuit Voltage (Voc)

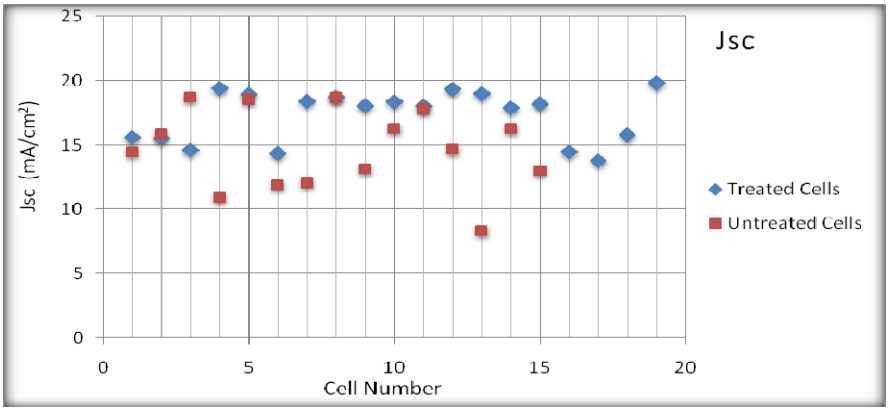

Figure 3.3 short-Circuit Current (Jsc)

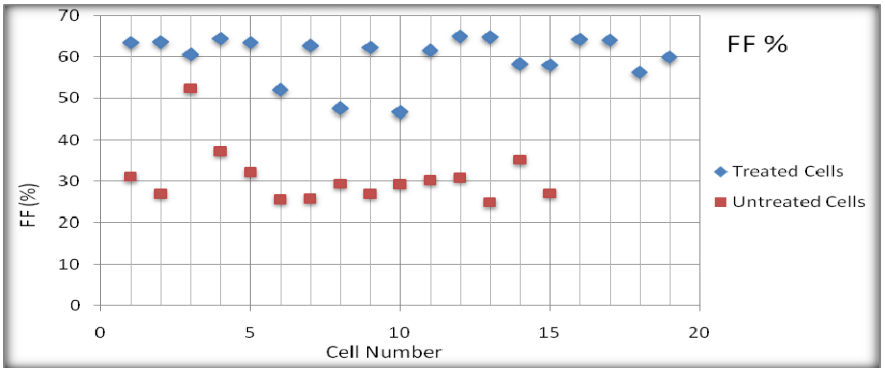

Figure 3.4 Fill Factor (%)

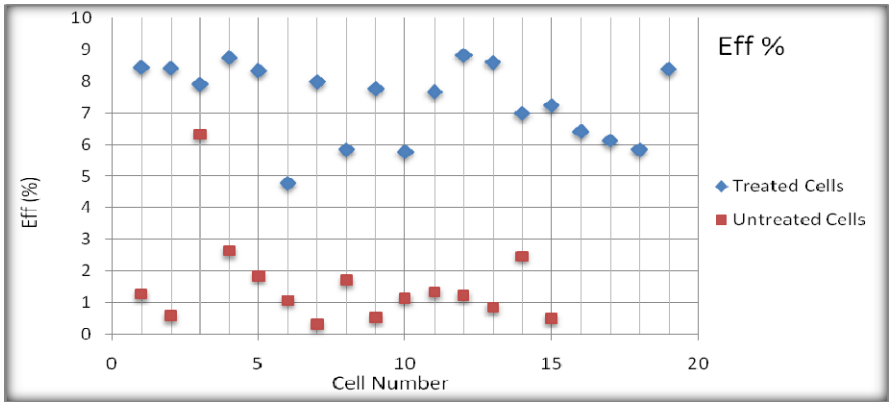

Figure 3.5 Efficiency (%)

Using the I-V measurement to characterize the CdTe devices, we have seen that the electrochemically treated (with aniline) samples gave a better/higher performance. As shown in Figure 3.2, 3.4, and 3.5 we can clearly see that the performance has increased in open-circuit voltage, fill-factor and efficiency, respectively. However, the short-circuit current remains the same as was expected. In the 15 samples that were not treated there is ample evidence for the formation of an electrical contact between the TCO and metal layers, while in the 19 treated this contact has been prevented.

Further work is in progress to optimize this process and to explore other potential monomers.